Conf-9109221--5

Fermi National Accelerator Laboratory

FNAL/C--92/24-E

DE92 010481

QCD and Jets at CDF

B. Flaugher for the CDF Collaboration

Fermi National Accelerator Laboratory
P.O. Box 500, Batavia, Illinois 60510

January 1992

Published Proceedings *XXI International Symposium on Multiparticle Dynamics*, Wuhan, China, September 23-27, 19991.

Disclaimer

FERMILAB-CONF-92/24-E
CDF/PUB/JET/PUBLIC/1672

QCD and Jets at CDF

CDF Collaboration
Presented by Brenna Flaugher*
Fermi National Accelerator Laboratory
Batavia, Illinois U.S.A. 60510

ABSTRACT

A summary of QCD results from the Collider Detector at Fermilab is presented. Comparisons are made to leading order, $O(\alpha_s^2)$, and next-to-leading order, $O(\alpha_s^3)$, parton level calculations and to leading logarithm shower Monte Carlo results.

1. Introduction

Many tests of QCD have been performed with the Collider Detector at Fermilab (CDF). This paper presents a summary of the QCD results using jet data collected during the 1988-1989 running of the Fermilab $\sqrt{s}$= 1.8 TeV proton-antiproton collider. The inclusive jet spectrum, dijet mass and angular distribution are compared to leading order, $O(\alpha_s^2)$, QCD predictions. Comparisons to next-to-leading order, $O(\alpha_s^3)$, QCD calculations are presented for the inclusive jet cross section and for the dijet angular distribution. A study of the jet shape is described and comparisons are made to the $O(\alpha_s^3)$ parton level calculations as well as to shower Monte Carlo results. Studies of 3-jet, 4-jet and 5-jet events are described. The inclusive photon cross section and the photon-jet angular distribution have been measured and are compared to theoretical predictions.

2. Jet Identification at CDF

2.1. The CDF detector

The CDF detector has been described in detail elsewhere.[1] Briefly, the detector elements used in these analyses are the central tracking chamber, which is in a 1.4 Tesla solinoidal magnetic field, and the electromagnetic and hadronic calorimeters. The tracking extends to $|\eta| \approx 1.2$ (η =-$ln(tan\theta/2)$, where θ is the polar angle with respect to the beam) with a charged particle momentum resolution of roughly $\delta P_t/P_t^2 \approx 0.0015 GeV/c^{-1}$. The calorimetry covers the range of $|\eta| \leq 4.2$

The calorimeter is segmented into "towers" which each have an electromagnetic and hadronic component. The towers are projective, pointing back to the center of the

*Supported by the U.S. Dept. of Energy, contract number DE-AC02-76CH03000
Published Proceedings XXI International Symposium on Multiparticle Dynamics, Wuhan, China, September 23-27, 1991.

interaction region. The angular segmentation of the towers in η is 0.1-0.2. In ϕ, the azimuthal angle around the beam, the tower sizes are 0.26 radians for $|\eta|$ <1.1 and 0.087 radians for 1.1< $|\eta|$ <4.2.

This segmentation is smaller than the typical size of a jet. Figure 1 shows a typical jet event in the CDF calorimeter. The shading of the towers represents the electromagnetic energy (dark) and the hadronic energy (light). The height of the towers is proportional to the E_T deposited.

2.2. Data samples

The majority of the jet data was collected using a trigger which required a localized cluster of energy in the calorimeter. To span a large range in E_T and cross section, thresholds of 20, 40, and 60 GeV were used. The lower E_T triggers were prescaled by 1/300 and 1/30 respectively. This data sample was used for the inclusive jet cross section, the jet shape and the dijet measurements.

In addition, to avoid possible biases associated with an online cluster requirement, a trigger based on the total E_T deposited was also used. A scalar sum over calorimeter towers was performed, and events having more than 120 GeV total E_T were passed. This data sample was used for the multi-jet (3-,4-, and 5-jet) analyses.

The photon data was selected by requiring an isolated cluster in the electromagnetic calorimeter with E_T above 23 GeV, and with no charged particle tracks pointing towards the cluster.[2]

The total integrated luminosity for the 1988-1989 data sample was 3.9 pb^{-1}.

2.3. Jet Cluster Algorithm

CDF uses a cone algorithm for jet identification,[3] where the radius of the cone is defined as R=$\sqrt{\Delta\eta^2 + \Delta\phi^2}$. In Fig. 1, the circle around the energy deposition indicates the boundary of the cluster cone. The energy and momenta of all calorimeter towers within the cone are summed to give a single four-vector for each jet. The sums run over the towers in the cone which have E_T >100 MeV. A cone size of R=0.7 is used in all CDF jet analyses unless otherwise indicated.

3. Inclusive Jet Cross Section

For many years, leading order, $O(\alpha_s^2)$, predictions for the inclusive jet cross section have existed (see, for example, Ref. 4). These calculations have a large uncertainty due to the uncertainty in the choice of renormalization scale. Recently, next-to-leading order, $O(\alpha_s^3)$, calculations have been performed.[5-7] In these calculations, the 3-jet matrix elements are incorporated into the calculation of the inclusive cross section through the use of a parton merging algorithm. The algorithm used in Ref. 5 is similar to the CDF cluster algorithm. A cone is defined around each parton with a radius of R=$\sqrt{\Delta\eta^2 + \Delta\phi^2}$. If two partons fall within a cone, then the E_T of the "jet" is defined as the sum of the E_T of the partons.

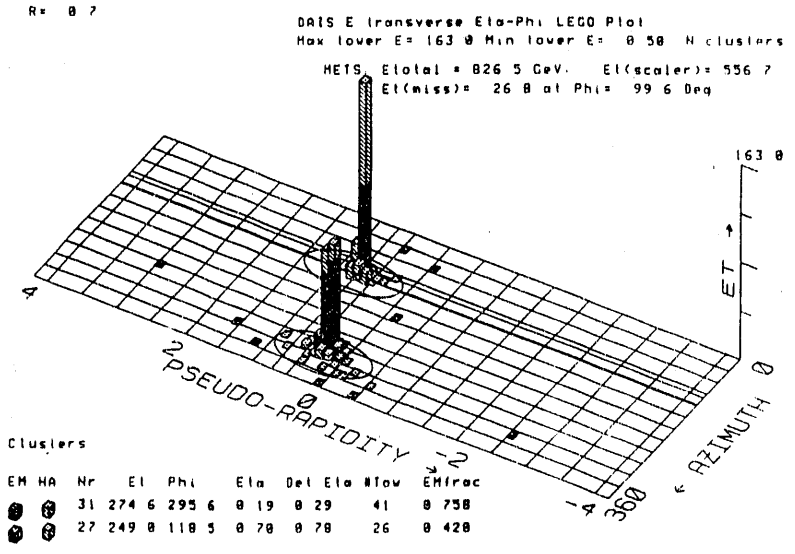

Figure 1: A jet event in the CDF calorimeter with the clustering cone indicated.

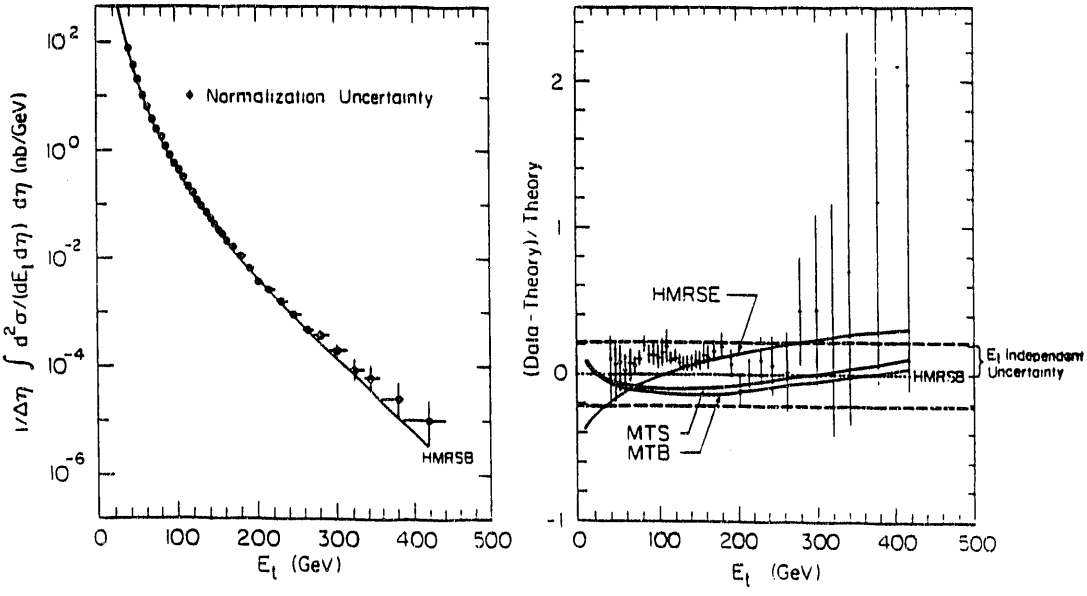

Figure 2: CDF inclusive jet cross section compared to the $O(\alpha_s^3)$ QCD prediction for a cone size of 0.7.

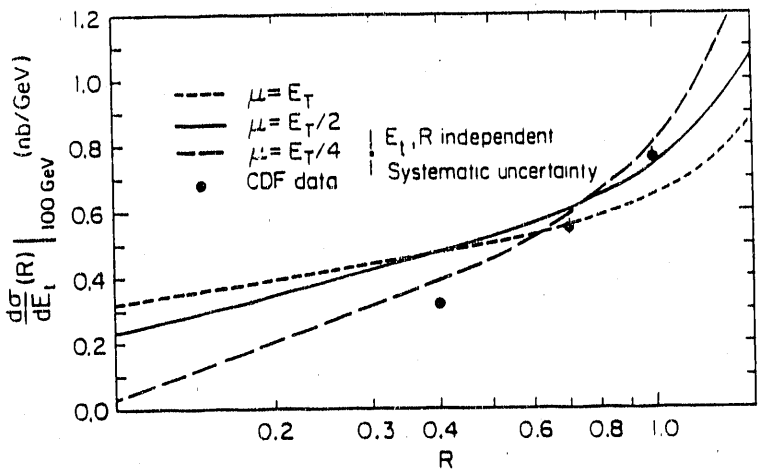

Figure 3: Dependence of the inclusive jet cross section on the clustering cone size for jets with $E_T \approx$100 GeV, compared to $O(\alpha_s^3)$ predictions.

Figure 2 shows the inclusive jet cross section compared to the next-to-leading order QCD prediction.[5] The normalization of the theory to the data is absolute. For this analysis the jets were restricted to the central region, $0.1 < |\eta| < 0.7$, of the CDF detector. The data has been corrected for detector effects and for the underlying event energy. No attempt has been made to correct for the effect of energy loss outside the cone since this is, in principle, accounted for in the $O(\alpha_s^3)$ calculation. Studies of the energy scale and resolution show that the uncertainty in the measurement is dominated by uncertainty in the energy scale. For high energy jets, jets with E_T larger than 80 GeV, the uncertainty on the cross section is typically 22% and is independent of E_T . Below 80 GeV the uncertainty in the cross section is as high as 60% due to systematic effects associated with the jet energy resolution, combined with the uncertainty in the absolute energy scale. As discussed in detail in reference 8, these uncertainties are smaller than previous measurements[9] and, combined with the improvements in the theoretical calculations, allow a more precise test of QCD.

In addition to reducing the dependence on the choice of renormalization scale, the $O(\alpha_s^3)$ calculation predicts, at the parton level, a dependence of the cross section on the clustering cone size. This is not possible with the leading order parton level calculations. Figure 3 shows the inclusive jet cross section for 100 GeV jets as measured for 3 different cone sizes and compared to $O(\alpha_s^3)$ predictions for different renormalization scales.[5]

4. Jet Shape

A measurement of the jet shape provides another test of QCD. Both the leading logarithm shower Monte Carlo programs, such as HERWIG[10] and PYTHIA,[11] and the $O(\alpha_s^3)$ calculation[5] can be compared to the data. For this measurement,[12] charged particle tracks were used since they provide better spacial and momentum resolution

for single particles. The centroid of the calorimeter cluster is taken as the center of the jet. The charged particle P_T density is measured in a cone, of radius R, around the cluster centroid. The jet shape is defined in terms of the fractional P_T density, normalized by the total number of jets, N, and by the total charged particle P_T within a cone of 1.0:

$$Fractional P_t = \frac{P_t(R)}{P_t(R=1.0)},$$

where

$$P_t(R) = \frac{1}{N}\sum_1^N \int_0^R \frac{dP_t}{dr} dr.$$

Figure 4 shows a plot of the fractional P_T as a function of the cone radius for central ($0.1 < |\eta| < 0.7$) jets with E_T in the range 95-120 GeV. The curves for $O(\alpha_s^3)$ calculations with different renormalization scales are shown, as well as the result for the HERWIG shower Monte Carlo. The agreement between the $O(\alpha_s^3)$ calculation and the data is surprisingly good considering this is a parton level calculation and no fragmentation effects have been added. The leading logarithm Monte Carlo also shows very good agreement with the data.

The E_T dependence of the jet shape has been measured and provides another test of QCD. To minimize the uncertainties in the theory and in the measurement, the E_T dependence is represented in terms of the charged particle P_T within a cone of radius 0.4 divided by the charged particle P_T within a cone of radius 1.0. Figure 5 shows this for the data, the $O(\alpha_s^3)$calculation and for two shower Monte Carlo models. The data is seen to fall between the predictions. The parton level calculation predicts fatter jets (less fractional P_T within the center of the jet) and the shower Monte Carlo models predict narrower, more collimated jets. The trend in the data towards narrower jets with increasing jet E_T is seen with both types of model.

5. Dijet Variables

The cross section for dijet events can be written in terms of the mass, M_{JJ}, the center-of-mass scattering angle, θ^*, and longitudinal boost of the dijet system, $\eta_{boost} = (\eta_1 + \eta_2)/2$, where η_1 and η_2 are the pseudorapidities of the two highest E_T jets.[13] The dijet mass of an event is calculated using the four-vectors of the leading two jets. The scattering angle is related to η_1 and η_2 by the equations $\eta^* = (\eta_1 - \eta_2)/2$ and $\cos\theta^* = \tanh\eta^*$. In the comparisons to theoretical predictions, the angular distribution is plotted in terms of the variable $\chi = e^{2|\eta^*|}$. For t-channel exchange, which dominates at large η^* , the $dN/d\chi$ spectrum is expected to be flat and thus insensitive to smearing effects.

To obtain the best mass resolution for the dijet mass spectrum, the rapidities of the leading two jets are restricted to the region $|\eta| < 0.7$. For the angular distribution,

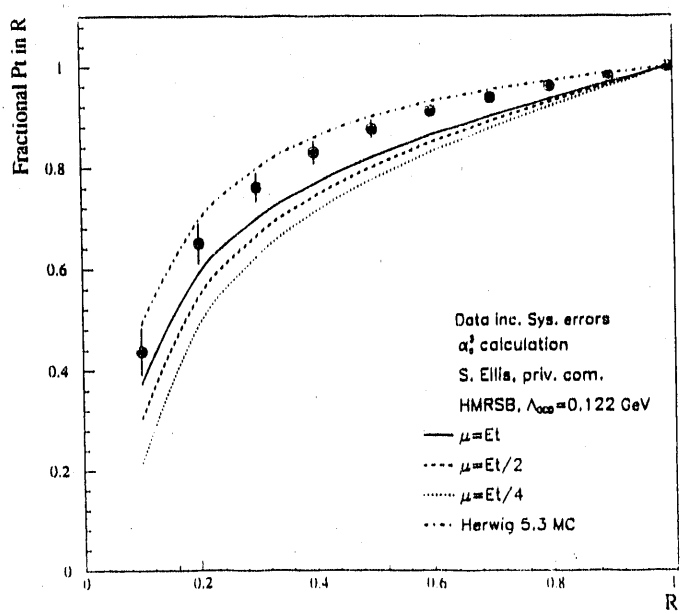

Figure 4: Fractional P_T within a cone of radius R for jets with E_T in the range 95-120 GeV.

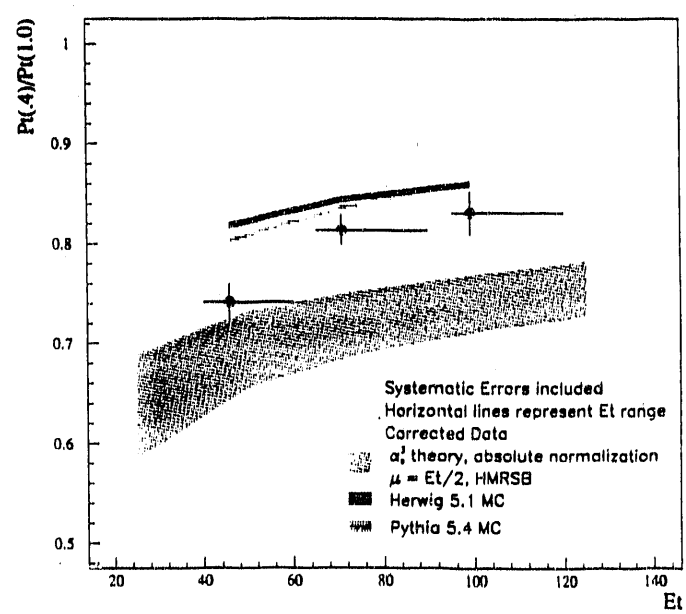

Figure 5: E_T dependence of the jet shape compared to parton level and shower Monte Carlo predictions.

where the extension to high values of η^* (χ) is more important than mass resolution, cuts requiring $|\eta_{boost}| < 0.75$ and $|\eta^*| < 1.6$ are imposed. These cuts more than double the angular range of the previous CDF measurement.[13] To ensure a fully efficient trigger over this larger angular range, the data is divided into mass windows of $240 < M_{JJ} < 475$ GeV, $475 < M_{JJ} < 550$ GeV and 550 GeV $< M_{JJ}$.

The data are corrected for detector effects such as nonlinear calorimeter response to low energy particles and for energy lost in cracks between detectors. Recent theoretical calculations include the effect of energy lost outside the jet cone, although there is still an uncertainty associated with underlying event energy. In order to present the data in a manner which is independent of the assumptions about the underlying event and out-of-cone energy, we do not attempt to correct for these effects.

Fits of the dijet mass spectrum to LO QCD have been discussed in Ref. 14 for a variety of renormalization scales and structure functions (DFLM, DO, EHLQ, HMRS, and the four Morfin-Tung sets). To summarize, for a cone size of 1.0, all structure functions fit the data well (40-60% confidence level) except EHLQ2 (21-25%), and the results are almost independent of the choice of scale. With a cone size of 0.7, all of the fits give confidence levels less than 6%. Figure 6 shows the range of $O(\alpha_s^2)$ QCD predictions compared to the CDF data. In this analysis, the parton level theoretical predictions are modified (smeared) by the effects of the detector resolution and energy scale and then compared to the data. $O(\alpha_s^3)$ calculations for a cone size of 0.7 have recently become available[15] and an early study indicates some improvement in the agreement between data and theory.

In the comparison of the dijet angular distribution to the theoretical calculations, fits are performed in which the normalization is a free parameter. With this approach we are sensitive to the shape of the $dN/d\chi$ distribution. Acceptance corrections are derived by comparing the shape of the angular distribution before and after a detector simulation. By varying the relative energy scales in different detector regions, upper and lower bounds representing the uncertainty in the acceptance corrections are derived. The data is corrected with the nominal, upper, and lower acceptance corrections and then fit to the theory. The range in the confidence levels represents the systematic uncertainty in the measurement.

Figure 7 shows the acceptance corrected data compared to $O(\alpha_s^2)$ and $O(\alpha_s^3)$ calculations[15] for HMRSB structure functions and with $O(\alpha_s^2)$ QCD for the Morfin-Tung sets. The theoretical curves are plotted with the best-fit normalization. Table 1 summarizes the results of the fits for the predictions. Four sets of Morfin-Tung structure functions were tested (S, B1, B2 and E); they gave the same confidence levels to within 2%.

6. Multi-jets

Events with more than two jets are predicted by QCD and provide a test of the higher order calculations. For 3-jet events, the variables under study at CDF are the

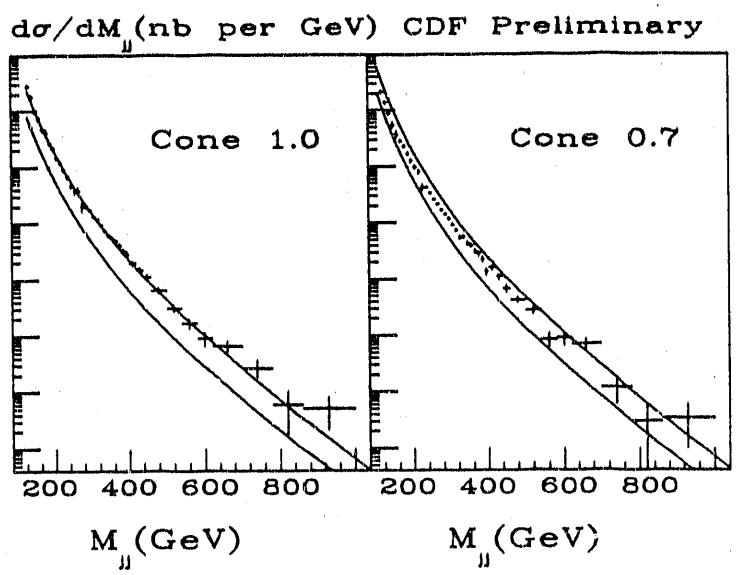

Figure 6: Dijet mass spectrum compared to QCD predictions for cone sizes of 0.7 and 1.0.

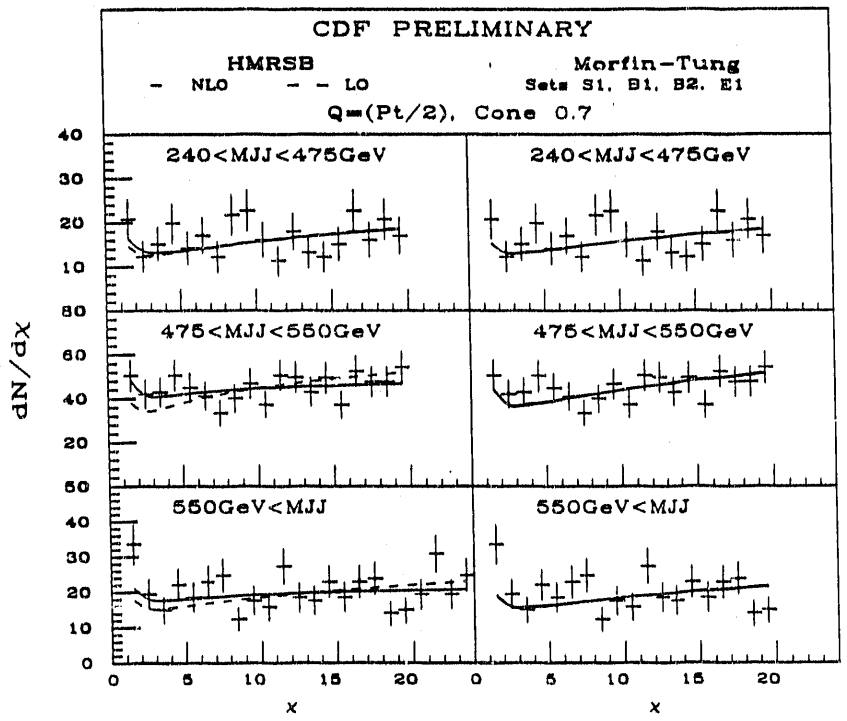

Figure 7: Dijet angular distribution compared to leading order and next-to-leading order QCD predictions.

Table 1: $O(\alpha_s^2)$ and $O(\alpha_s^3)$ theory compared to the CDF dijet angular distribution. The range in confidence levels (C.L.) represents the systematic uncertainty. Preliminary.

Structure function	Mass (GeV)	$O(\alpha_s^2)$C.L. (%)	$O(\alpha_s^3)$C.L. (%)
Morfin-Tung	240-475	37-60	-
HMRSB	240-475	31-53	41-60
Morfin-Tung	475-550	33-78	-
HMRSB	475-550	11-48	73-78
Morfin-Tung	>550	0.4-15	-
HMRSB	>550	$\leq$10	6-15

fractions of the maximum possible energy carried by each of the jets:

$$x_i = \frac{2E_i}{M_{3jet}},$$

where M_{3jet} is the 3-jet mass, i=3 refers to the highest energy jet and i=5 refers to the lowest energy jet in the center-of-mass frame.

Figure 8 shows a Dalitz plot and projections of energy fractions x_3 and x_4. The upper and lower corners on the right side of the Dalitz plot correspond to the infrared and collinear divergences of the 3-jet matrix elements, respectively. Cuts have been imposed to avoid these regions in both the theory and experiment. The projections are compared to the QCD predictions and to 3-body phase space. QCD is clearly preferred over phase space and shows a good fit to the data.[16]

While theory and experimental measurements show good agreement with the jet data, possible new phenomena could show up at high energies which might not have jet-like structure. To expedite the examination of the highest E_T (hottest) events at CDF, a cut of 400 GeV on the total scalar E_T was used to select events from the 120 GeV E_T data sample. This resulted in 279 events after backgrounds such as cosmic rays and double interactions were removed. Comparisons of many variables were made to the HERWIG Monte Carlo plus a full detector simulation and good agreement was observed. Figure 9 shows the total E_T spectrum and Fig. 10 shows the multijet mass of 2-jet, 3-jet, 4-jet and 5-jet events for the data (points) compared to the theoretical predictions (histograms). A complete description of this analysis is presented in reference 17.

7. Photons

Photons produced directly from the hard collision provide a probe of the gluon structure functions and an energy measurement which is free from the effects of fragmentation. Two approaches have been used by CDF for the detection of direct photons.

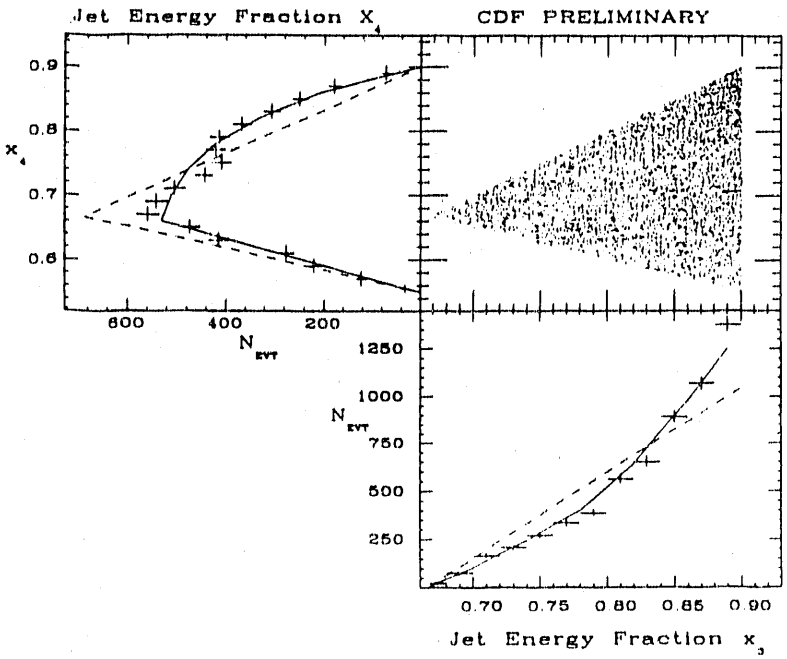

Figure 8: Dalitz plot for 3-jet events at CDF compared to QCD and phase space predictions.

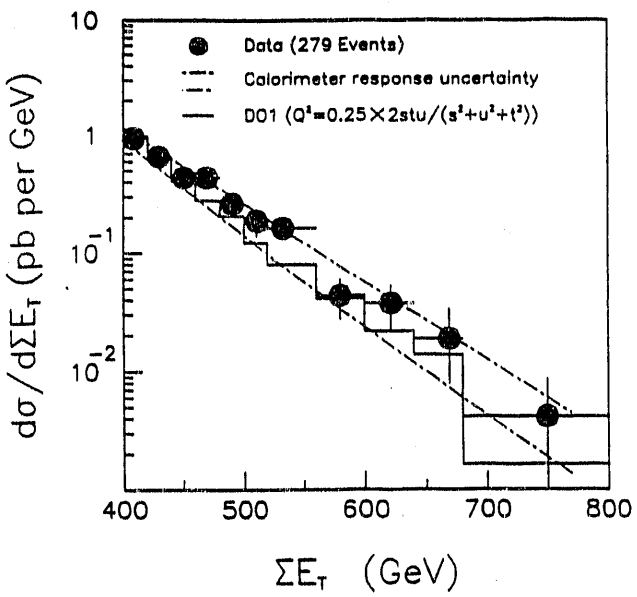

Figure 9: Total E_T spectrum for the highest E_T events compared to the HERWIG shower Monte Carlo with full detector simulation.

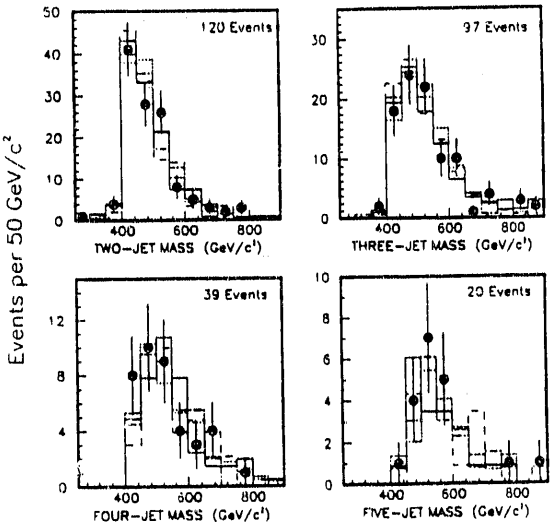

Figure 10: Multi-jet masses as observed in the highest E_T events, compared to the HERWIG shower Monte Carlo with full detector simulation.

The first method uses shower profiles as measured in strip chambers which are embedded at shower maximum (6 radiation lengths) in the central electromagnetic calorimeter. Comparison of the shower profiles from the data with shower profiles from test beam electrons allows the separation of photons from the background, which is mainly π^os. For P_T $<\approx$35 GeV, the two photons from a π^o decay will be far enough apart to produce distinct bumps in the transverse profile. At higher P_T the two photons from a π^o decay are indistinguishable from a single photon.

A second method is used to extend the P_T range of the inclusive photon cross section measurement. A known fraction of photons and π^os convert in the material between the tracking chamber and the electromagnetic calorimeter and thus, a statistical subtraction of the π^o background can be performed. For the analysis of the 1988-1989 data, the mass in the outer shell of the central tracking chamber was used as a converter. This corresponded to roughly 18% of a radiation length.

Figure 11 shows the P_T spectrum derived from the combination of the two methods.[2] The theoretical predictions are all next-to-leading order calculations and the renormalization scale is P_T . The data seems to have a steeper slope at low P_T than the theoretical predictions.

The effect of higher order terms and bremsstrahlung diagrams are under study. At present, the range in the predictions from different choices of renormalization scale and the disagreement between theory and data in the low P_T region, preclude the separation of the effects of different gluon structure functions.

In addition to the photon inclusive cross section, the photon-jet angular distribution provides a probe of the propagator in the proton-antiproton collisions. QCD

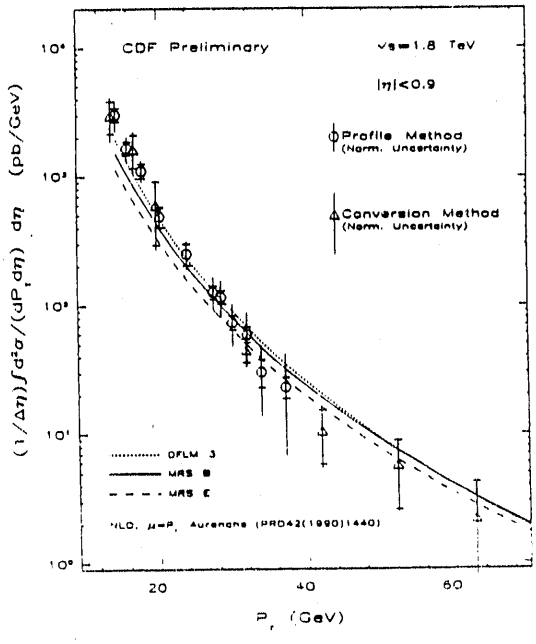

Figure 11: The inclusive photon cross section as measured at CDF compared to next-to-leading order calculations.

predicts that the jet-jet cross section is dominated by Rutherford-like t-channel gluon exchange (spin 1). The photon-jet final state is expected to be relatively flat since it is dominated by t-channel quark exchange (spin 1/2). This is directly reflected in the angular distribution.

For the photon-jet data, the variables η^* and $\cos\theta^*$ are defined using the pseudorapidity of the photon, η_γ, and the pseudorapidity of the jet, η_{jet}, which results from a vector sum of the jets which fall in a 120° cone opposite to the photon direction in ϕ:

$$\eta^* = (\eta_\gamma - \eta_{jet})/2$$

and

$$\cos\theta^* = \tanh\eta^*.$$

To avoid uncertainties associated with the measurement of the jet energy, the invariant mass of the photon-jet system is calculated using the P_T of the photon and η^*:

$$M_{\gamma,jet} = 2P_{t,\gamma}cosh\eta^*.$$

To ensure uniform acceptance, cuts were made on $M_{\gamma,jet}$ and on η^*. The value $M_{\gamma,jet}$ ranged from 57-94 GeV, with a maximum value of $|\eta^*| = 1.1$.

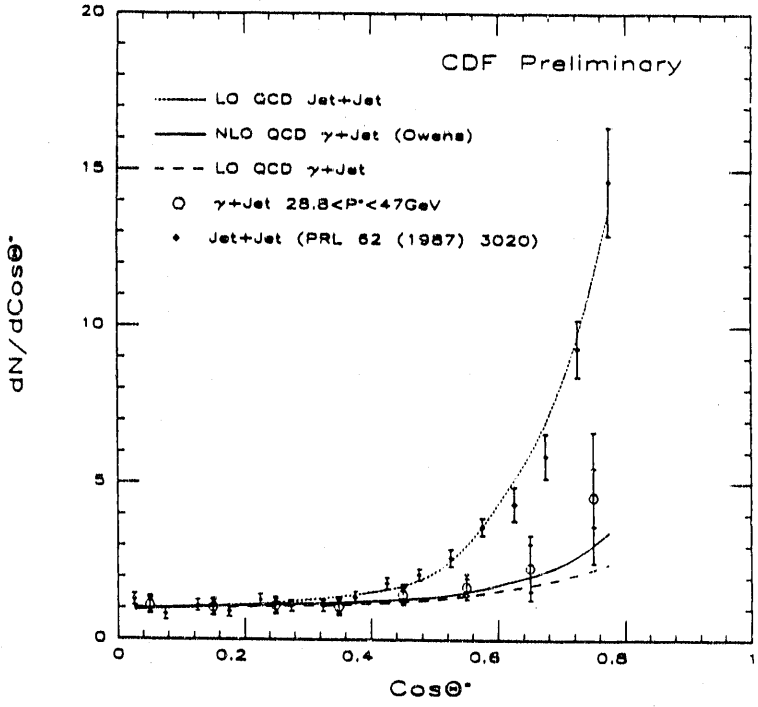

Figure 12: Photon-jet angular distribution compared to dijet angular distribution and to leading order and next-to-leading order QCD predictions.

Figure 12 shows photon-jet angular distribution compared to leading order and next-to-leading order QCD calculations.[2] The dijet angular distribution as previously measured by CDF has also been included since it was measured at low mass ($M_{jj} \geq$148 GeV) and thus is closer than the current dijet data to the mass used in the photon-jet measurement. Although the statistics are limited, the photon-jet predictions are clearly preferred by the photon-jet data over the dijet data and the dijet QCD predictions.

8. Conclusions

Many tests of QCD have been preformed and good agreement between the data and the theoretical predictions has been observed. We look forward to collecting new data in the near future.

References

1. F. Abe et al (CDF Collaboration), Nucl. Inst. and Meth. A271 (1988) 387.
2. CDF Collaboration, presented by R.M.Harris, FERMILAB-CONF-91/236-E.
3. B.Flaugher, K. Meier, FERMILAB-CONF-90/248-E.
4. For example: E. Eichten, I. Hinchliffe, K. Lane and C. Quigg, Rev. Mod. Phys. 56, 4, Oct. 1984.
5. S. Ellis, Z. Kunszt and D. Soper, Phys. Rev. D 40(1989) 2188;Phys.Rev.Lett.64 (1990) 2121.

6. R. Ellis and J. Sexton, Nucl. Phys. B 269(1986)445.
7. F. Aversa et al., Phys. Lett. B 210 (1988) 225.
8. F. Abe et al (CDF Collaboration), FERMILAB-PUB-91/231-E, Aug. 1991;to be published in Phys. Rev. Lett.
9. F.Abe et al.,(CDF Collaboration) Phys. Rev. Lett. 62, (1989) 613.
10. G. Marchesini and B.R. Webber, Nucl. Phys. B310 (1988) 461.
11. H.U. Bengtsson, T.Sjostrand, Computer Phys. Comm. 46 (1987) 43; T. Sjostrand, Computer Phys. Comm. 39 (1986) 347.
12. CDF Collaboration, presented by N. Wainer, FERMILAB-CONF-91/249-E.
13. F.Abe et al.,(CDF Collaboration) Phys. Rev. Lett. 62 (1989) 3020.
14. P. Giannetti (CDF Collaboration), FERMILAB-CONF-91/137-E.
15. D. Soper, private communication.
16. F. Abe et al (CDF Collaboration), FERMILAB-PUB-91/181-E, Aug. 1991;to be published in Phys. Rev. D.
17. F. Abe et al (CDF Collaboration), FERMILAB-PUB-91/283-E, Oct.1991;to be published in Phys. Rev. D.

END

DATE
FILMED
5/07/92